Dynamic uniaxial extension of elastomers at constant true strain rate

Jean-Christophe Petiteau, Ramzi Othman, Pierrick Guégan, Hervé Le Sourne, Erwan Verron

Dynamic uniaxial extension of elastomers at constant true strain rate

Jean-Christophe Petiteau [a], Ramzi Othman [a,c], Pierrick Guégan [a], Hervé Le Sourne [b], Erwan Verron [a]

[a] *LUNAM Université, Ecole Centrale de Nantes, GeM, UMR CNRS 6183, BP 92101, 44321 Nantes cedex 3, France*
[b] *LUNAM Université, Institut Catholique d'Arts et Métiers (ICAM), 35 avenue du champ de Manoeuvres, 44470 Carquefou, France*
[c] *Mechanical Engineering Department, Faculty of Engineering, King Abdulaziz University, P.O. Box 80248, Jeddah 21589, Saudi Arabia*

Elastomers are widely used for damping components in various industrial contexts because of their remarkable dissipative properties: they can bear severe mechanical loading conditions, i.e., high strain rates and large strains. Depending on the strain rate, the mechanical response of these materials can vary from purely rubber-like to glassy. In the intermediate strain rate range (1-100/s), uniaxial extension experiments are classically conducted at constant *nominal* strain rate. We present here a new experimental methodology to investigate the mechanical response of soft materials at constant *true* strain rate in the intermediate strain rate range. For this purpose, the displacement imposed on the specimen by the tensile machine is an exponential function of time. A high speed servo-hydraulic machine is used to perform experiments at strain rates ranging from 0.01 to 100/s. A specific specimen is designed in order to achieve a uniform strain field (and thus a uniform stress field). Furthermore, an instrumented aluminium bar is used to measure the applied force; which overcomes the difficulties due to dynamic effects. Simultaneously, a high speed camera enables the measurement of strain in the sample using a point tracking technique. Finally, the method is applied to determine the stress-strain curve of an elastomer for both loading and unloading responses up to a stretch ratio $\lambda = 2.5$; the influence of the true strain rate on both stiffness and dissipation of the material is then discussed.

Keywords:
True strain rate
Experimental technique
Intermediate strain rate
Elastomer
Strengthening

1. Introduction

Because of their remarkable dissipative properties, elastomers are widely used as damping components in industry, especially to absorb shock. Indeed, they can undergo severe mechanical loading conditions, i.e. both large strain and strain rates. Nevertheless, because of their viscoelastic nature, the mechanical response of these materials may vary from purely rubber-like to glassy depending on the strain rate, as shown by Yi *et al.* [1] and Sarva *et al.* [2] among others.

In order to design industrial components, it is of major importance to measure the sensitivity of the mechanical response to strain rate. At very low and very high strain rates, the conventional tensile machines and the Hopkinson pressure bar set-up [3], respectively, are classically used. However, there is no consensus of opinion on the methodology that should be undertaken for intermediate strain rates. Hoo Fatt and co-workers [4,5] proposed a modified Charpy test in order to achieve homogeneous strain and stress fields as quickly as possible by applying a tensile force on both sides of the specimen with the help of a system of pulleys and cables. Roland *et al.* [6] followed a similar method and modified a drop weight machine. Even if these solutions are of interest, they necessitate high accuracy in the design of pulleys and cables in order to achieve sufficient

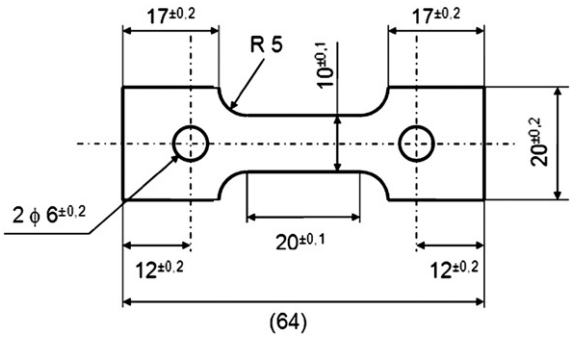

Fig. 1. Sample design.

synchronization of the forces applied at specimen extremities: the delay between loading instants must be insignificant compared with test duration. Recently, Othman *et al.* [7] proposed a hybrid servo-hydraulic machine for intermediate strain rate testing. Namely, the conventional piezoelectric transducer is replaced by a three-gauge instrumented elastic bar in order to capture transient effects; the three strain-gauge signals are then analysed by a wave separation technique as proposed in Refs. [8,9] and already applied to the Hopkinson pressure bar set-up [10,11].

In the present paper, we are interested in testing rubberlike materials at constant true strain rates and large strains, in order to better understand the behaviour of the material depending on the strain rate. It is recognized that the cam plastometer set-up is well-suited to test materials at constant true strain rates [12]. Nevertheless, it requires complex equipment and has never been used for soft materials. Thus, we propose here to use a standard servo-hydraulic machine. In the range of intermediate strain rate, i.e. from 0.01 to 100/s, a technique similar to that described in Ref. [7] is considered. Moreover, specimens are designed to rapidly achieve uniform strain and stress states to avoid the use of a correction method as proposed in [13,14].

2. Method

2.1. Material and sample

The major objective of our experiments is to demonstrate the ability to perform constant true strain rate tension tests for a wide range of strain rate while achieving large strains. As the measurement of strain cannot be direct, we cannot use a regulation loop to prescribe a constant true strain rate in the central part of the sample. Therefore, the feed-back loop must be considered in terms of displacement. For this reason, we developed a specific sample for the present test. Classical dumbbell samples cannot be used for large strain rates because the sample

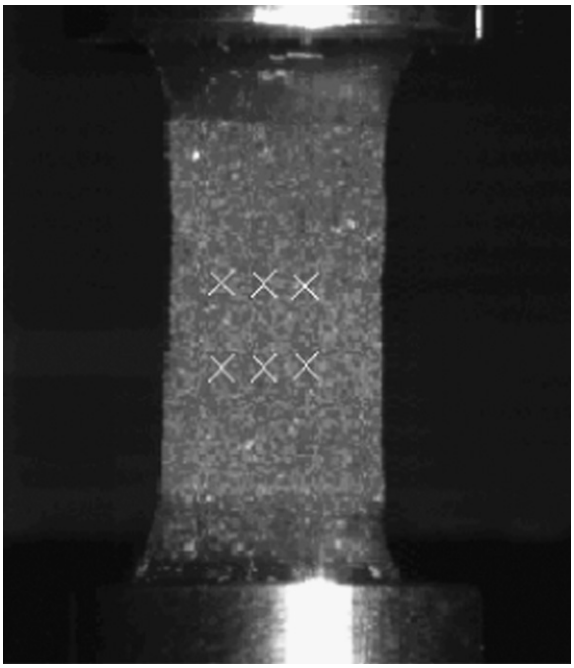

Fig. 2. Position of the points used for tracking.

centre is stretched more than the zone near the grips and, as rubber response is non-linear, it becomes difficult to predict the strain field in different parts of the specimen. Thus, the sample section must be constant between the clamps to ensure the best possible homogeneity of both strain and strain rate fields (see Fig. 1). The section of the sample was defined in order to have stresses high enough to be measured by the force transducer, and the length of the sample was defined in order to have a uniaxial test and, at the same time, to be able to apply the desired displacement speed depending on the machine used. The samples were obtained by water jet cutting.

Two different styrene butadiene rubbers (SBR) filled, respectively, with 20 and 40 phr of carbon black were considered; henceforth referred to as SBR20 and SBR40. The gauge (central part) is 20 mm long. Considering a wave velocity of some hundreds of metres per second, the time necessary to achieve homogeneous stress and strain is some hundreds of micro-seconds. In the most limiting case, i.e., for strain rates of about 100/s, the elongation of the sample is only a few percent before attaining homogeneous fields in the sample. Moreover, the sample is strained less than 1% before reaching stress and strain homogeneity at a strain rate of about 10/s. Finally, the stress and strain in the specimen are legitimately assumed homogeneous; and then the stress can be deduced from the measurement of the boundary (extremity) force.

Table 1
Parameters used for the camera.

Strain rate of the test (/s)	0.01	10	100
Frame frequency (f/s)	20	10000	16000
Resolution (pixels^2)	256 × 1024		

Table 2
Frequencies used for the gauge signals.

Strain rate of the test (/s)	0.01	10	100
Acquisition frequency (kHz)	0.1	100	500

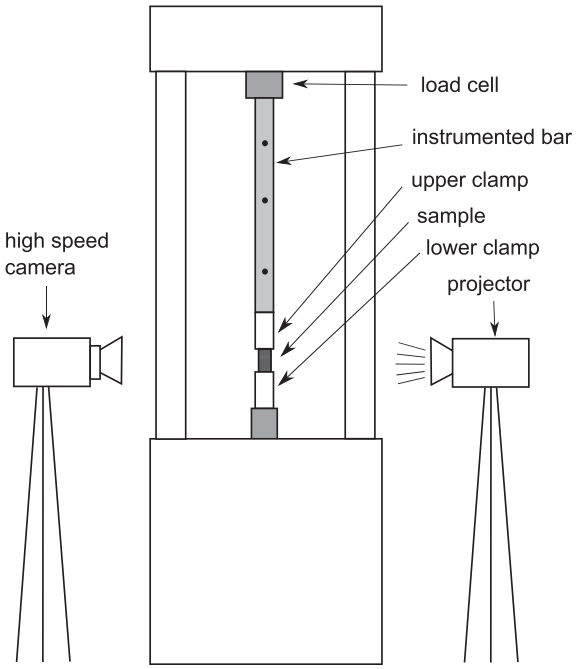

Fig. 3. Experimental set-up.

2.2. Machine and loading conditions

The experimental device is a high speed hydraulic machine (MTS 819). The displacement of the cylinder is controlled by a computer, using a LABVIEW program specially developed for these experiments.

Performing tensile experiments at constant true strain rate means that the symmetric part of the velocity gradient **D** remains constant. We assume that the deformation is homogeneous in the sample, and denote **F** the deformation gradient. Noting, $\overrightarrow{V}(\overrightarrow{X},t) = \overrightarrow{v}(\overrightarrow{x},t)$ the velocity field, two different velocity gradients can be defined: the first with respect to the undeformed configuration, i.e. the nominal velocity gradient,

$$grad_{\overrightarrow{X}}\overrightarrow{V}(\overrightarrow{X},t) = \dot{\mathbf{F}}(\overrightarrow{X},t) \tag{1}$$

and the second with respect to the current configuration, i.e. the true velocity gradient,

$$grad_{\overrightarrow{x}}\overrightarrow{v}(\overrightarrow{x},t) = \mathbf{L}(\overrightarrow{x},t) \tag{2}$$

The relationship between these two quantities is

$$\mathbf{L} = \dot{\mathbf{F}}\mathbf{F}^{-1} \tag{3}$$

Eliminating the rotation contribution of the motion, the strain rate tensor is the symmetric part of **L**:

$$\mathbf{D} = \frac{1}{2}\left(\mathbf{L} + \mathbf{L}^{T}\right) \tag{4}$$

For uniaxial tension, denoting $\overrightarrow{e_1}$ the stretching direction and $\overrightarrow{e_2}$ and $\overrightarrow{e_3}$ the transverse directions, the deformation gradient of an incompressible material reduces to

$$\mathbf{F} = \lambda\overrightarrow{e_1}\otimes\overrightarrow{e_1} + \frac{1}{\sqrt{\lambda}}\left(\overrightarrow{e_2}\otimes\overrightarrow{e_2} + \overrightarrow{e_3}\otimes\overrightarrow{e_3}\right) \tag{5}$$

where λ is the stretch ratio, i.e. the ratio of the deformed and undeformed lengths l/l_0. Then, the true strain rate is simply

$$\mathbf{D} = \frac{\dot{\lambda}}{\lambda}\overrightarrow{e_1}\otimes\overrightarrow{e_1} - \frac{\dot{\lambda}}{2\lambda}\left(\overrightarrow{e_2}\otimes\overrightarrow{e_2} + \overrightarrow{e_3}\otimes\overrightarrow{e_3}\right) \tag{6}$$

To ensure that **D** remains constant, the stretch ratio must be written as $\lambda = e^{\alpha t}$, instead of $\lambda = \alpha t$ as it is commonly prescribed for uniaxial extension experiments at constant engineering strain rate. Finally, the deformation gradient reduces to

$$\mathbf{F} = e^{\alpha t}\overrightarrow{e_1}\otimes\overrightarrow{e_1} + e^{-\frac{\alpha t}{2}}\left(\overrightarrow{e_2}\otimes\overrightarrow{e_2} + \overrightarrow{e_3}\otimes\overrightarrow{e_3}\right) \tag{7}$$

In order to prescribe a constant true strain rate, we must control the displacement of the lower grip of the stretching machine such as $u = l_0(e^{\alpha t} - 1)$. One can note that for small strain, i.e. $\lambda \approx 1$, the two strain rates $\dot{\mathbf{F}}$ and **D** coincide.

2.3. Measurement of strain and stress

Strain was measured by a point tracking technique. A random speckle was painted on the sample and each

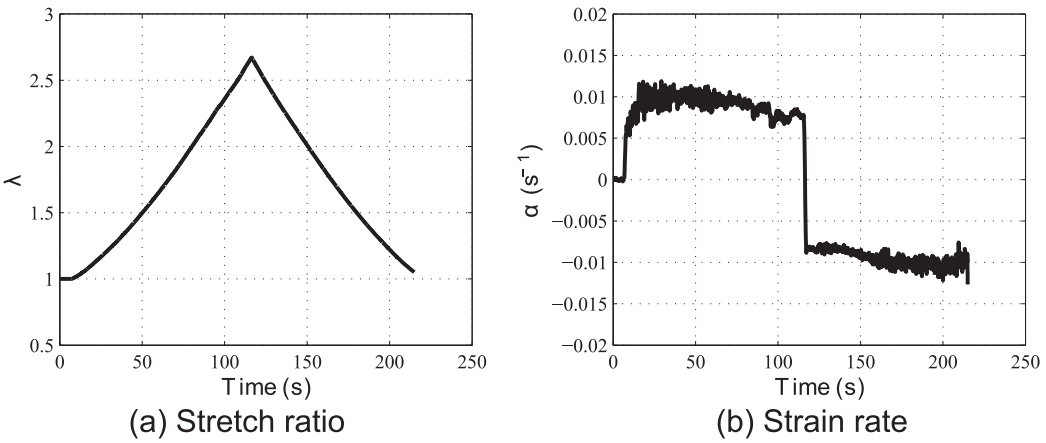

Fig. 4. (a) Stretch ratio and (b) true strain rate at 0.01/s.

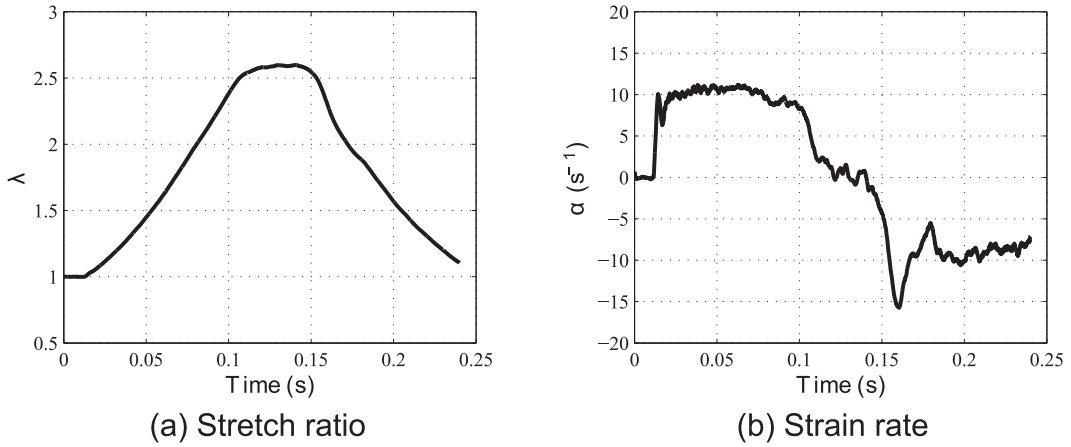

Fig. 5. (a) Stretch ratio and (b) true strain rate at 10/s.

test was recorded using a high-speed camera (PHOTRON FASTCAM SA1), the parameters of which are given in Table 1.

Note that the sample must be illuminated with a spotlight to properly record images. As shown in Fig. 2, the displacement of several points in the recorded images was determined by the point tracking software TEMA Automotive. Once the displacements were obtained, the time evolution of the longitudinal stretch ratio (in direction $\overrightarrow{e_1}$) was calculated in various points i of the sample

$$\lambda(t) = \frac{l(t)}{l_0} = \frac{X_2(t) - X_1(t)}{X_2(0) - X_1(0)} \tag{8}$$

where X is the coordinate in the $\overrightarrow{e_1}$-direction and the subscript 1 and 2 stand for close measurement points. Finally, the strain rate was deduced using Eq. (6). Note that the displacement along the transverse direction is very small and cannot be accurately determined with our point tracking technique.

As mentioned above, the stress field is assumed homogeneous. Thus, the stress is averaged by measuring the force at an extremity of the specimen. Here, two methods were considered to measure this force. The first consists of the use of a classical force cell. Nevertheless, as transient effects become increasingly significant as strain rate increases, large oscillations are observed on the force signals. To overcome this limitation, we considered a second method to measure the force. The servo-hydraulic machine was equipped with a second force transducer which is a tubular aluminium bar instrumented with three strain gauges. This method is inspired by the work of Othman *et al.* [7] but there are two differences. First, an aluminium tube rather than a steel rod was used here, in order to decrease both the stiffness and the section of the bar. In this way, the signal-to-noise ratio is increased, as suggested by Chen *et al.* [15], for soft materials. Second, the wave separation technique is not considered here; as the tube is 0.4 m long and the distance between gauges is about 0.15 m, the time for the wave to travel from one gauge to the other is about 30 μs, which is insignificant compared with the experiment duration. Thus, the tube can be considered as quasi-statically loaded, the signals of the three strain-gauges are averaged and, finally, the force is deduced considering the Young modulus and the section of the tube. Obviously, the accuracy of the method is also related to the acquisition frequency of the gauge signals; for the different strain rates they are given in Table 2.

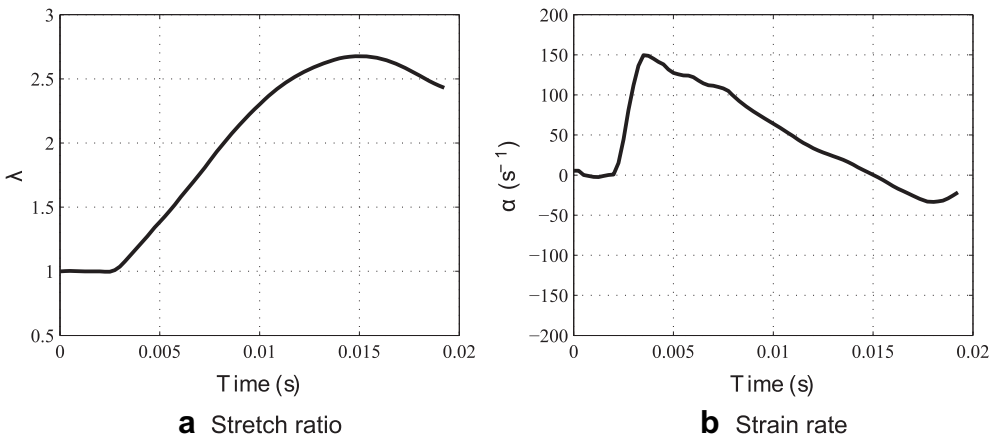

Fig. 6. (a) Stretch ratio and (b) true strain rate at 100/s.

Table 3
Average and standard deviation of the strain rate obtained.

Desired true train rate (/s)	0.01		10		100
	Load	Unload	Load	Unload	Load
Average true strain rate (/s)	0.0091	−0.0095	9.9	−9.4	84
Standard deviation	0.0012	0.0009	0.93	1.93	42

To summarize, a sketch of the experimental set-up is presented in Fig. 3.

2.4. Experimental procedure

For a given sample, the procedure was as follows. First, five uniaxial extension cycles up to $\lambda = 2.6$ at a strain rate of 0.01/s were performed the day before the experiment to remove the Mullins effect. Second, after placing the painted sample in the grips, the initial length of the specimen, i.e. the length between grips, was measured and entered as an input in the LABVIEW program. Third, the strain rate was chosen and the function displacement versus time was calculated by the LABVIEW program. Finally, the test started. All the tests were made at ambient temperature.

3. Results and discussion

3.1. Measurement of strain and strain rate

As mentioned above, for each test and for each time, the stretch ratio at different positions in the sample was measured. The value of the stretch ratio at a given time is simply the mean value over the sample. Nevertheless, measured signals are noisy, and we used the local polynomial interpolation smoothing technique to obtain a relevant signal [14]. For each point of the stretch versus time curve, 15 points before and 15 points after it were considered; the curve composed by these 31 points was then fitted with a second order polynomial function; finally the value of this function at the measurement point was considered as the stretch. With this method, the stretch versus time curve is sufficiently smooth to calculate the true strain rate α by derivation. Figs. 4–6 present the stretch ratio versus time and true strain rate versus time curves for 0.01/s, 10/s and 100/s respectively.

In order to evaluate the method, we calculated the average true strain rate over loading and unloading parts of the cycles for each desired strain rate, and the corresponding standard deviation; the results are given in Table 3.

These results and the strain rate versus time curves in Figs. 4–6(b) confirm that the set-up is well-designed and permits constant true strain rates experiments ranging from 0.01 to 10/s.

During experiments at 100/s, the delay between the prescribed and the recorded displacements is more important than at lower strain rates. Moreover, only the loading part of the cycle has been prescribed in order to prevent the clamps from colliding during unloading. In fact, at 100/s we reached the limitations of the machine and we were not able to perform perfect constant true strain rates experiments. Note, however, that the strain rate recorded is not so far from the prescribed value (see Fig. 6(b)), and that the experiment leads to valuable information because we are able to record all the values during the test.

3.2. Measurement of stress

A hardware low-pass filter with a cut-off frequency of 10 kHz was used for the tests at 0.01/s because higher frequencies do not bring any information at this strain rate. For 10 and 100/s, no hardware filter has been used in order to record the maximum of data. Figs. 7–9 present (a) the data measured by the force cell, (b) the data measured by the three strain gauges and (c) the filtered signal for $\alpha = 0.01$/s, $\alpha = 10$/s and $\alpha = 100$/s, respectively. As shown in Fig. 7(a), and as expected, the force cell gives relevant results for low strain rates. On the contrary, as the strain rate increases, noise and perturbation in signals are observed (see Fig. 8(a)): natural frequencies of the force cell are excited in the intermediate strain rate range [7]. On the other hand, the signal recorded by the strain gauges placed on the aluminium bar gives good results at intermediate strain rates (see Figs. 8 and 9(b)) but deviates for low strain rates (see Fig. 7(b)). This deviation is due to heating of the bar because of the spotlight used to illuminate the sample.

Finally, for small strain rates (0.01/s), we only considered the force cell to determine the stress. At intermediate strain rates (10-100/s), we only considered the gauge instrumented bar technique. As there is no noticeable time shifting between the three curves, the mean value over the three gauges is considered instead of using a wave separation technique. A similar smoothing technique to that

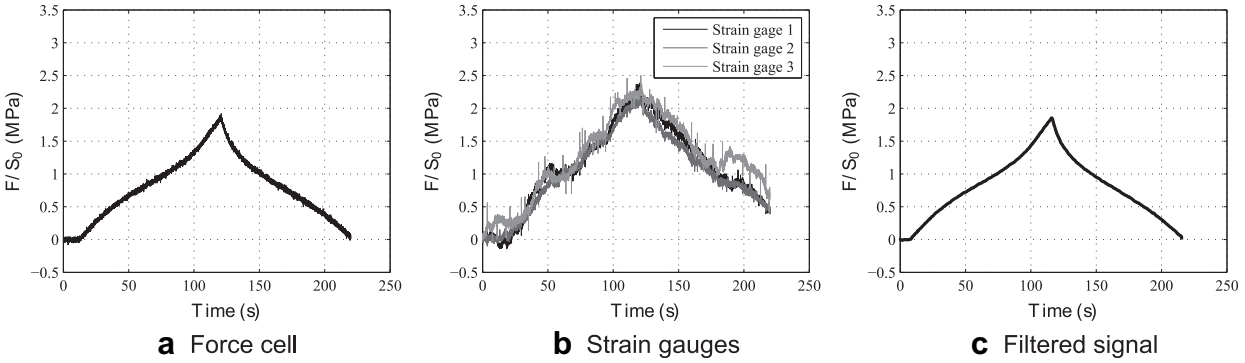

Fig. 7. Engineering stress versus time for a strain rate $\alpha = 0.01$/s: (a) data measured by the force cell, (b) data measured by the three strain gauges, (c) filtered signal.

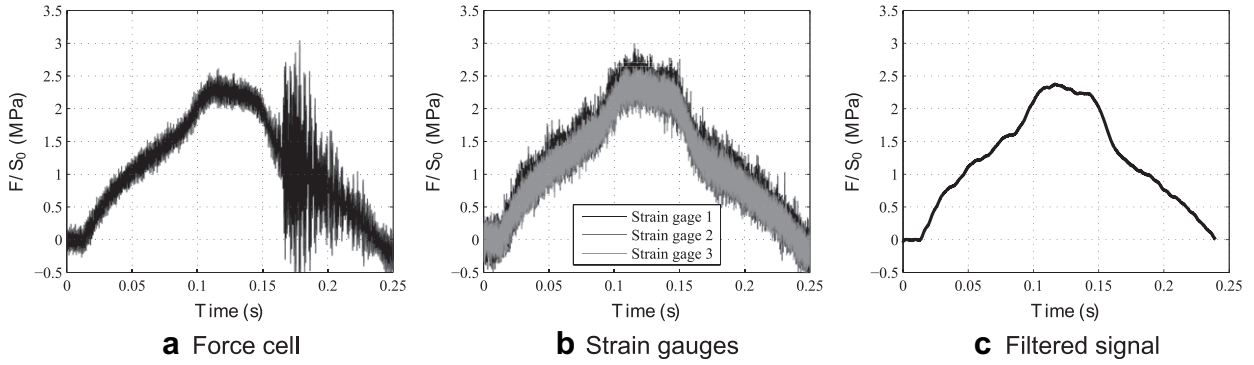

Fig. 8. Engineering stress versus time for a strain rate $\alpha = 10$/s: (a) data measured by the force cell, (b) data measured by the three strain gauges, (c) filtered signal.

considered for strain measurement was used to smooth the curves; in this case, 35 points before and 35 points after the considered point were taken into account. The final stress versus time curves are shown in Figs. 7–9(c).

3.3. Determination of the stress-strain response

In sections 3.1 and 3.2, respectively, we succeeded in measuring stretch and stress versus time. However, the time line is not the same for both measurements because the acquisition hardware is different. To synchronize the measurements, the starting time ($t = 0$ s) is set by considering that the maximum stress and strain occur at the same time. Moreover, as acquisition frequencies differ for stretch and stress, the time steps are different. Hence, the stretch and stress are interpolated with respect to the same time line. Figs. 10 and 11 present the stress-stretch relationship of SBR20 and SBR40, respectively, at several strain rates. Both materials experience an important strengthening as strain rate increases. Moreover, as shown in Fig. 12(a), the initial stiffness, i.e. the slope of the stress-stretch curve at small strain, is more important for large strain rates: the initial stiffness of SBR20 at 100/s is more than three times the stiffness at 0.01/s, and the initial stiffness of SBR40 at 100/s is at least five times larger than that at 0.01/s. Furthermore, Figs. 10 and 11 show that the hysteresis loop is larger for large strain rates. Even if we are unable to perform the unloading part of the cycles at 100/s, the reader can easily guess that the hysteresis loop at 100/s is larger than at 10 and 0.01/s. The larger the hysteresis loop, the more important the dissipation; therefore both materials exhibit dissipative properties that increase with the strain rate, as shown in Fig. 12(b): the dissipation at 10/s is at least one and a half (1.5) times the dissipation observed under quasi-static loading conditions.

3.4. Discussion

The main objective of this study was to achieve constant true strain rate in uniaxial extension experiments of soft materials for large strains and intermediate strain rates.

- For strain rates up to 10/s, this aim is completely fulfilled, as shown is Figs. 4–5(b).
- For 100/s, the task was found to be more difficult. The strain rate measured during loading changes from 80 to 150/s during the first 7 ms of the test, which shows that we are able to attain a good order of magnitude for the strain rate. The major drawback of the largest strain rate test, i.e. at 100/s, is the difficulty in unloading the specimen. Consequently, no data are available to estimate dissipation at this strain rate.

Our methodology has been applied to two SBR compounds. The results highlight an important sensitivity of their response to strain rate:

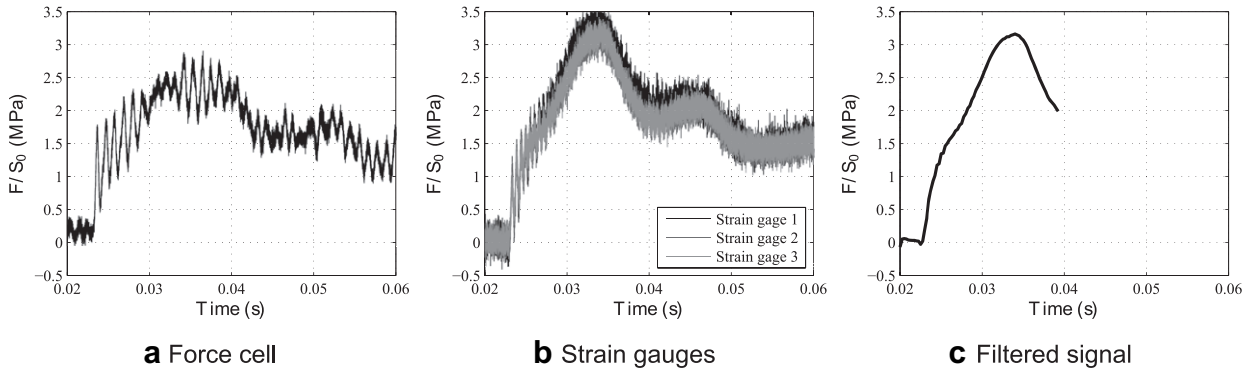

Fig. 9. Engineering stress versus time for a strain rate $\alpha = 100$/s: (a) data measured by the force cell, (b) data measured by the three strain gauges, (c) filtered signal.

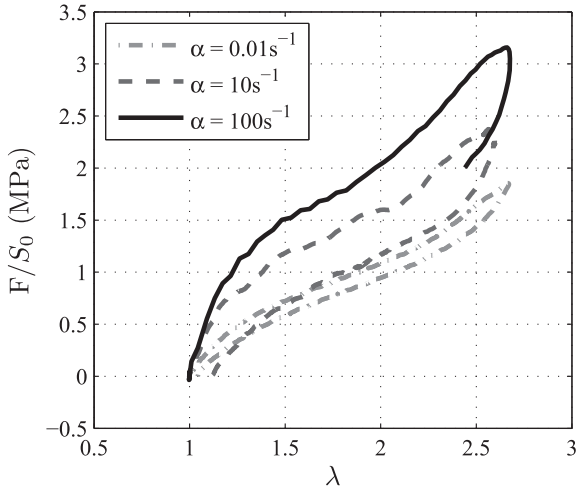

Fig. 10. Engineering stress with respect to stretch ratio for different strain rates for SBR20.

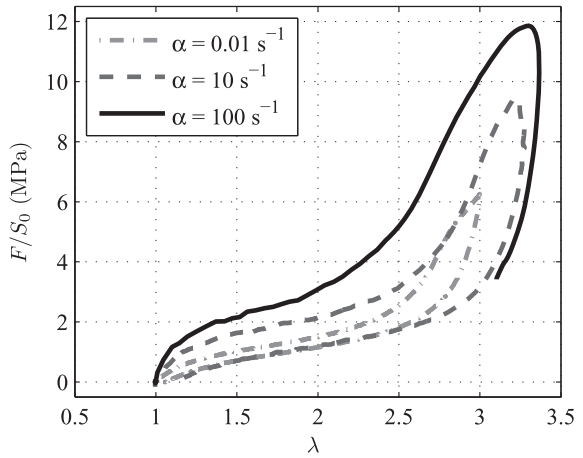

Fig. 11. Engineering stress with respect to stretch ratio for different strain rates for SBR40.

- Namely, both materials exhibit strengthening as the strain rate increases; which is in good agreement with the observations of Hoo Fatt and Ouyang [5]. Similar results were also obtained for polyurea [2,11].
- As the strain rate increases, the hysteresis loop between the loading and the unloading parts of the cycle becomes larger, and dissipation increases for both materials. There are no similar results in the literature, so no comparison can be proposed for the dependence of dissipation on strain rate.

4. Conclusions

We propose here a method to perform uniaxial extension experiments at constant true strain rate and large strains. The approach uses a standard high speed servo-hydraulic machine. It necessitates the use of specially designed samples with constant section between the clamps in order to obtain homogeneous strain and stress fields. The relative displacement of the grips is an exponential function of time. A tracking point technique is applied to measure the stretch in the sample. To measure the stress, two types of sensors are used: a classical force cell for low strain rates and a three strain gauge tubular aluminium bar for intermediate strain rates.

The methodology leads to almost constant true strain during both loading and unloading for experiments at true strain rates lower than 10/s. However, for 100/s the measured true strain rate varies from 80 to 150/s. Indeed, the order of magnitude is obtained but it is not sufficiently precise.

The stress-stretch curve of two SBR materials for a complete cycle, i.e. loading and unloading parts, is determined for strain rates up to 10/s, but only the loading part of the response is obtained for 100/s. The results show that both SBRs exhibit strengthening as the strain rate increases and an increase in the size of hysteresis loop. To put these results in perspective, it would be interesting to compare them with tests performed at constant nominal strain rate.

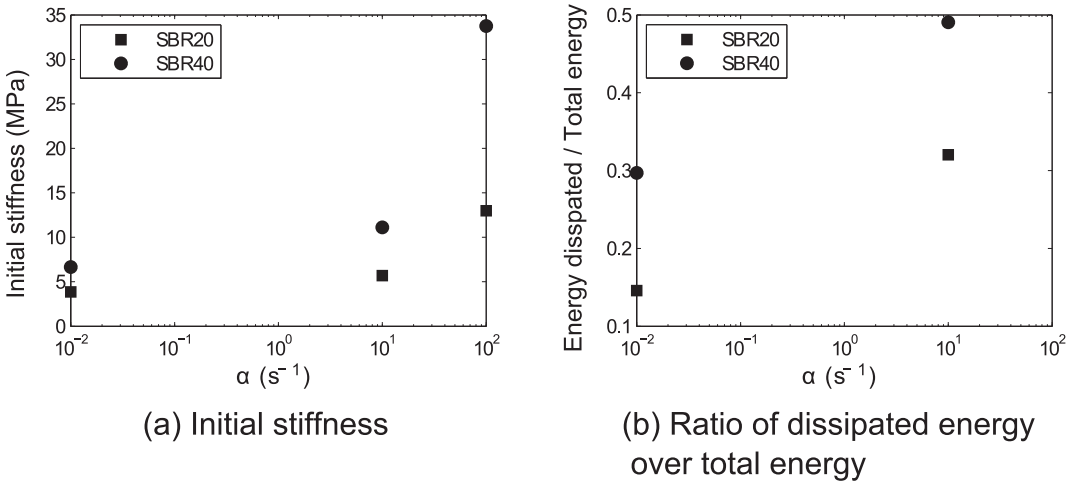

Fig. 12. (a) Initial stiffness and (b) dissipation depending on the strain rate.

Acknowledgements

The authors highly acknowledge DGA and DCNS for their financial support and would like to thank F. Pasco (Ecole Centrale de Nantes) for his help in the experimental work.

References

[1] J. Yi, M. Boyce, G. Lee, E. Balizer, Polymer 47 (1) (2006) 319–329.
[2] S.S. Sarva, S. Deschanel, M.C. Boyce, W. Chen, Polymer 48 (8) (2007) 2208–2213.
[3] G. Gary, Techniques de l'Ingénieur BM 7 (176) (2001) 1–10. 16.
[4] M.S. Hoo Fatt, I. Bekar, J. Mater. Sci. 39 (23) (2004) 6885–6899.
[5] M.S. Hoo Fatt, X. Ouyang, Mechanics Mater. 40 (1–2) (2008) 1–16.
[6] C.M. Roland, J.N. Twigg, Y. Vu, P.H. Mott, Polymer 48 (2) (2007) 574–578.
[7] R. Othman, P. Guégan, G. Challita, F. Pasco, D. Lebreton, Int. J. Impact Eng. 36 (2009) 460–467.
[8] R. Othman, M.N. Bussac, P. Collet, G. Gary, C.R. Acad, Sci. Série IIb 329 (2001) 369–376.
[9] M.N. Bussac, P. Collet, G. Gary, R. Othman, J. Mechanics Phys. Solids 50 (2002) 321–349.
[10] R. Othman, G. Gary, Exp. Mech. 47 (2007) 295–299.
[11] J. Shim, D. Mohr, Int. J. Impact Eng. 36 (2009) 1116–1127.
[12] ASM Handbook, vol. 8, 2000, pp. 429–446.
[13] S. Aloui, R. Othman, A. Poitou, P. Guégan, S. El-Borgi, Mech. Res. Comm. 35 (2008) 236–244.
[14] R. Othman, S. Aloui, A. Poitou, Polym. Test. 29 (2010) 616–623.
[15] W. Chen, B. Zhang, M.J. Forrestal, Exp. Mech. 39 (1999) 80–85.